Investigating the Relationship between Infrared Spectra of Shared Protons in Different Chemical Environments: A Comparison of Protonated Diglyme and Protonated Water Dimer

Sven Lammers and Markus Meuwly*

Department of Chemistry, University of Basel, Klingelbergstrasse 80, 4056 Basel, Switzerland

Received: August 17, 2006; In Final Form: December 30, 2006

The energetics, dynamics, and infrared spectroscopy of the shared proton in different chemical environments is investigated using molecular dynamics simulations. A three-dimensional potential energy surface (PES) suitable for describing proton transfer between an acceptor and a donor oxygen atom is combined with an all-atom force field to carry out reactive molecular dynamics simulations. The construction of the fully dimensional PES is inspired from the established mixed quantum mechanics/molecular mechanics treatment of larger systems. The "morphing potential" method is used to transform the generic PES for proton transfer along an $O\cdots H^+\cdots O$ motif into a three-dimensional PES for proton transfer in protonated diglyme. Using molecular dynamics simulations at finite temperature, the gas phase infrared spectra are calculated for both species from the Fourier transform of the dipole moment autocorrelation function. For protonated diglyme the modes involving the H^+ motion are strongly mixed with other degrees of freedom. At low temperature, the $O\cdots H^+\cdots O$ asymmetric stretching vibration is found at 870 cm^{-1}, whereas for $H_5O_2^+$ this band is at 724 cm^{-1}. As expected, the vibrational bands of protonated diglyme show no temperature dependence whereas for $H_5O_2^+$ at $T = 100$ K the proton transfer mode is found at 830 cm^{-1}, in good agreement with 861 cm^{-1} from very recent molecular dynamics simulations.

I. Introduction

The transfer of protons in chemically (acid−base chemistry, proton conducting wires) and biologically (enzymatic reactions) relevant systems is of fundamental importance for a variety of processes. Early models go back to Grotthus in the 1800s, which view proton transfer (PT) in a liquid as a shuttling process between reorienting molecules.[1] Despite the tremendous progress in experimental techniques, it was only possible for a long time to *indirectly* infer proton transfer in the ground state and in the gas phase, because it is a transient process. This is in contrast to experiments in the condensed phase where it is possible to investigate hydrogen bonds using infrared spectroscopy because of the larger number densities.[2] For the electronically excited state, PT is a much better characterized process, in particular because double resonance and molecular beam techniques were developed and matured.[3−5] With the advent of tunable, high-luminosity light sources in the mid-infrared (free electron lasers or optical parametric oscillators), the use of direct absorption spectroscopy to characterize a strongly bound protonated system in the gas phase has become possible. The first observation of the protonated water dimer in the region between 600 and 1900 cm^{-1} is an example for this recent success.[6] Additional experiments on the same and related systems have provided further information about the vibrational spectroscopy of the shared proton.[7,8] Alternatively, vibrational predissociation spectroscopy of mass-selected, rare gas-solvated $H_5O_2^+(Ar)_n$ and $H_5O_2^+(Ne)_n$ has been used to characterize the molecular vibrations of $H_5O_2^+$ as a function of the degree of solvation n.[9] This study has provided some evidence that the asymmetric OH*O stretching frequency is around 1000 cm^{-1}. However,

because complexation with a Ne atom lowers the symmetry of the system, it is possible that some bands split. This is observed in the experiment but could not be reproduced by several computational techniques and the authors were not prepared to make a firm assignment, in particular, of the identity and origin of the lower frequency component of the doublet.[9]

Recently, it has been suggested that from the assignment of vibrational bands in $H_5O_2^+$, the vibrational spectrum of a proton shared between two oxygen atoms for a series of $AO\cdots H^+\cdots OA$ motifs (where A forms the chemical environment for the bridging proton transfer motif; $A = H_2$ for $H_5O_2^+$) can be inferred. In particular, the asymmetric stretch vibration in protonated diglyme ([diglyme-H]$^+$) has been assigned by visually comparing the spectrum with that of $H_5O_2^+$.[8] A possible justification for the hypothesis that the vibrational spectra of the shared proton in $H_5O_2^+$ and in [diglyme-H]$^+$ are related, is that the potential energy surfaces that govern proton transfer between two oxygen atoms in $H_5O_2^+$ and [diglyme-H]$^+$ are topologically related. In the present work we test this hypothesis by using state-of-the art interaction potentials designed to describe proton transfer.

Over the past few years, computational and theoretical investigations of proton transfer in isolated or solvated systems have attracted considerable interest.[10−23] Some of these studies used empirical potentials,[11−13,16,18] whereas others treated the electronic energy with Car−Parrinello or related approaches.[17,19,20,24,25] Examples include the proton transfer dynamics along a chain of water molecules[16,19,24,26] or a mixed water−ammonia chain.[17] Other work was concerned primarily with the proper treatment of the nuclear dynamics using path integral[12,13,16,18] or basis set methods.[14] For $H_5O_2^+$ in particular computational studies have investigated the structure and

Shared Protons in Different Chemical Environments

J. Phys. Chem. A, Vol. 111, No. 9, 2007 **1639**

harmonic and anharmonic vibrations at various levels of sophistication.[21,23,27−30] They range from classical molecular dynamics (MD) simulations[23,28,30] to fully dimensional diffusion Monte Carlo (DMC) calculations.[29] Molecular dynamics simulations play a central role for the investigation of such systems because simulations at finite temperature are able to sample and characterize the properties of the system at configurations that are far from the equilibrium structure. In the present work this is important because we are interested in the dynamics of the proton transfer and the spectroscopic information derived from it. Furthermore, previous computational work showed that the vibrational spectrum of $H_5O_2^+$ is temperature-dependent[23,31] and the experiments are carried out at high laser power, which provides considerable amounts of internal energy to the species considered.[6−8] Contrary to high-resolution spectroscopic experiments in cold, supersonic expansions for which many successful bound state calculations exist,[32,33] the assignment of vibrational spectra for molecular species recorded at extreme (high laser power) conditions is likely to require alternative methods than those previously employed for high-resolution spectroscopic experiments.[32]

One of the difficulties in using molecular dynamics (MD) simulations to investigate the energetics, dynamics and spectroscopy involving reactive processes is that the potential energy functions are not suited to describe bond formation and bond breaking. For sufficiently small systems (several atoms) it is possible to calculate and fit a fully dimensional potential energy surface and to use it in MD simulations. For larger systems, such as protonated diglyme or proton transfer in a protein environment, this approach is not feasible because of the high dimensionality to describe the PES. On the other hand, the energy expression of a conventional force field, which is usually fitted to structural and spectroscopic data, is not suitable for investigating bond breaking and bond forming processes.[34,35] Possible extensions to describe reactive phenomena include mixed quantum mechanics/molecular mechanics calculations (QM/MM).[36−38] They decompose the system into a part that is directly involved in the reaction and treat it by quantum mechanics, whereas the rest of the system is treated by a molecular mechanics force field. Examples for the QM part are explicit ab initio techniques[39] or density functional theory, semiempirical treatments (e.g., AM1/PM3), empirical valence bond theory (EVB),[40] or approximate valence bond theory (AVB).[41] However, even in the QM/MM framework high level QM approaches are difficult to use for sufficiently long simulation times (several picoseconds up to nanoseconds) due to the large amount of computer time required for dynamical studies.

In the present work an approach inspired by mixed QM/MM calculations is used that combines a potential energy surface (PES), the QM part, suitable for describing the proton transfer between an acceptor and a donor atom with a force field, the MM part, for the remaining degrees of freedom. The three-dimensional PES is calculated at the MP2 level for $H_5O_2^+$ as a model system for proton transfer and then transformed to describe PT in protonated diglyme. Previous work has studied topological similarities of PESs calculated at different levels of ab initio theory[33,42,43] whereas in the present case the chemical environment motivates a relationship between the PESs ("morphing") via a transformation. In its original formulation, morphing was used to systematically modify an ab initio potential to fit experimental data. The procedure retains the general shape of the ab initio potential but allows, e.g., barrier heights and the absolute and relative depths and distances of
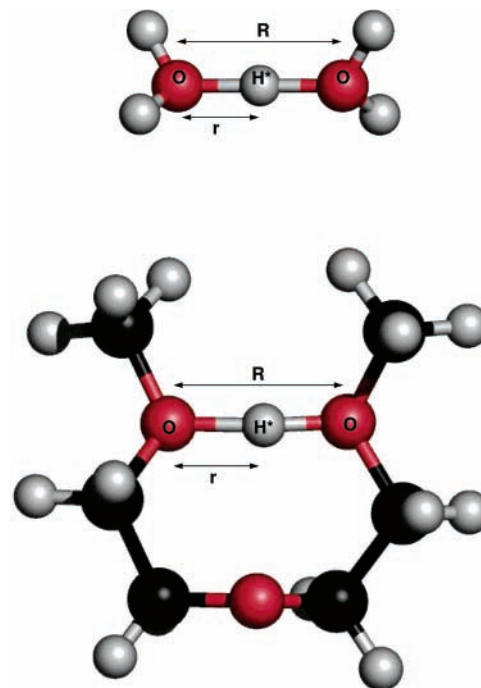
Figure 1. Minimum energy structures of (a) protonated water dimer at the MP2/6-311++G(d,p) level of theory and (b) protonated diglyme at the B3LYP/6-311++G(d,p) level of theory. The heavy−heavy distance (O···O) is R, and the hydrogen coordinate is r and the angle θ is the angle between the two. For the linear arrangement $\theta = 0°$. The transferring hydrogen/deuteron is labeled H*/D*.

potential minima to change. The first application showed that it is possible to transform an approximate PES (calculated at a lower level of ab initio theory) into a high quality PES that is capable of reproducing all experimental observables for Ne−HF to within spectroscopic accuracy.[33] Here, the morphing approach is used to transform a generic, high-quality, multidimensional PES for proton transfer in $H_5O_2^+$ to a PES that captures the energetics of proton transfer in protonated diglyme. The two PESs are then used in finite-temperature MD simulations which allows to exhaustively sample the multidimensional PES.

The work is organized as follows: in the next section the computational methods used are presented. Next, the dynamics and the infrared spectra for both protonated diglyme and $H_5O_2^+$ are analyzed and compared. Finally, the results are discussed and conclusions are presented.

II. Computational Methods

A. Intermolecular Interactions. In the following, the O···O (donor−acceptor) distance is R and the O−H* distance (separation of transferring hydrogen to the donor atom) is r. The angle θ is defined as the scalar product between the unit vectors $\hat{R}$ and $\hat{r}$ (see Figure 1). Ab initio calculations were carried out at the MP2/6-311++G(d,p) (for $H_5O_2^+$) and B3LYP/6-311++G(d,p) (for protonated diglyme) using Gaussian03.[44] For scanning the fully relaxed potential energy surfaces (PESs) in the collinear $\theta = 0°$ conformation of the PT motif, the (R, r) grid was defined by $R \in [2.2, 3.2]$ Å in increments of 0.1 Å and r between 0.8 Å and the midpoint between the two oxygen atoms in increments of 0.05 Å. For each geometry (R, r) all other coordinates were optimized, which finally leads to a relaxed PES. To describe the bending degrees of freedom in $H_5O_2^+$, further calculations were carried out at

TABLE 1: Parameter Set for the Fit of of the Proton Transfer Potentials in $H_5O_2^+$ (Eqs 2−7)

	$D_e(R)$		$\beta(R)$		$R_{eq}(R)$		k		c
p_1	141.902 kcal/mol	p_5	−0.977 Å^{-1}	p_7	357.171 Å	p_{10}	0.009 kcal/mol	p_{11}	35.621 kcal/mol/deg
p_2	2.229 Å^{-1}	p_6	1.348 Å^{-2}	p_8	3.393 Å^{-1}				
p_3	1.960			p_9	0.102 Å				
p_4	11.879 kcal/mol								

TABLE 2: Atom Types for $H_5O_2^+$ and Protonated Diglyme from the CHARMM22 Force Field[47]

$H_5O_2^+$		protonated diglyme	
atom type	atom number	atom type	atom number
H	H1···H5	H	H1···H15
O	O1, O2	C	C1···C6
		O	O2
		OH	O1, O3

angles $\theta = 11.98°$, $27.49°$, $43.10°$, and $58.73°$ on the same (R, r) -grid as for $\theta = 0$. This gives a total of 1265 points. The θ-grid was chosen for an efficient and stable representation of the angular dependence by Legendre polynomials and to describe internal rotation of the H_3O^+ molecule. However, for the present applications the angular dependence is sufficiently well described by a harmonic potential (as in a conventional force field) in θ, because reorientation phenomena are not of interest. To enhance the robustness of the fit in its short and long range R-region, very short (1.8 and 2.0 Å) and very long (4.0, 6.0, and 8.0 Å) O−O distances R were included in the fit for selected angular cuts. The data were fit using I-NoLLS, a program for interactive nonlinear least-squares fitting of the calculated energies to a functional form of the potential energy surface.[45]

For the MD simulations, the three-dimensional PES $V(R,r,\theta)$ was implemented into the CHARMM program. A fuller account of the implementation can be found in ref 46. The total electronic energy of the system (with coordinates $\vec{x}$) is decomposed into a part for the proton transfer motif ($V_{PT}(R,r,\theta)$) and the remaining degrees of freedom $\vec{y}$ of the system. Thus, the total interaction is written as

$$V(\vec{x}) = V_{PT}(R,r,\theta) + V_{MM}(\vec{y}) \qquad (1)$$

The resulting potential, eq 1, is called molecular mechanics with proton transfer (MMPT).

In a conventional MD simulation the bonds are defined at the beginning of a calculation and cannot be broken or formed subsequently. The present setup follows this standard procedure in that the hydrogen/proton (H*, see Figure 1) of interest is initially bonded to the donor D. However, during the simulation the functional form of $V_{PT}(R,r,\theta)$ (see below) is suited to describe the atom H* leaving D and binding to the acceptor atom A. Both D and A are usually bonded to other atoms, X, of the molecular framework. This involves angular (bonded) terms such as XDH*. Whenever H* attempts to transfer from D to A, such bonded terms are damped from the total energy and corresponding new terms (e.g., YAH*) are introduced in a smooth fashion. A switch function $f_{sw}(R,r)$ is used to turn the necessary terms on or off. For this, a sigmoid function $f_{sw}(R,r) = (1/2)(\tanh(a \cdot R(r-(R/2))) + 1)$ is chosen. With $a = 2$ Å^{-2}, f_{sw} yields 0.5 at the transition state and values close to 1 if H* is bound to D and 0 if H* is bound to A. Nonbonded terms are treated in an analogous manner. The above scheme is valid for symmetric systems (identical terms are removed and introduced on the D and A side, respectively).

For rapid evaluation of the energies and gradients, the functional form of $V(R,r,\theta)$ is chosen with some care.

To stabilize the fitting, it was found advantageous to express the potential energy surface as $V_{PT}(R,\rho,\theta)$ with $\rho = (r - r_{min})/(R - 2r_{min})$ and $r_{min} = 0.8$ Å. Thus, the coordinates of $V_{PT}(R,\rho,\theta)$ are R (D−A separation), ρ (position of H* relative to D for a particular R), and the angle θ. Overall, $V_{PT}(R,\rho,\theta)$ is given by

$$\begin{aligned} V_{PT}(R,\rho,\theta) = {} & D_{eq}(R)[1 - \exp(-\beta(R)(\rho - R_{eq}(R)))]^2 + \\ & D_{eq}(R)[1 - \exp(-\beta(R)(1 - \rho - R_{eq}(R)))]^2 - \\ & D_{eq}(R) + c + k\theta^2 \quad (2) \end{aligned}$$

where the parameters D_{eq}, β, and R_{eq} are functions of R and c and k are constants:

$$D_{eq}(R) = p_1(1 - \exp(-p_2R - p_3))^2 + p_4 \qquad (3)$$

$$\beta(R) = p_5 + p_6R \qquad (4)$$

$$R_{eq}(R) = p_7 \exp(-p_8R) + p_9 \qquad (5)$$

$$k = p_{10} \qquad (6)$$

$$c = p_{11} \qquad (7)$$

For protonated diglyme, the proton transfer motif is described with the same functional form of $V(R,\rho,\theta)$. However, its shape is modified through a transformation $(V(R,\rho,\theta) \rightarrow \tilde{V}(R,\rho,\theta))$ to capture the essential features of the relaxed PES from the B3LYP/6-311++G(d,p) calculations. For this, two morphing parameters were introduced, namely an energy scaling λ_1 $(V \rightarrow \lambda_1 V)$, and a distance scaling λ_2 $(R \rightarrow \lambda_2 R)$. The two parameters λ_1 and λ_2 are determined such as to reproduce the location of the minimum energy structure R_{min} calculated with B3LYP/6-311++G(d,p) and to better represent the flatter surface of protonated diglyme compared to that for $H_5O_2^+$ for large separations R. As mentioned above, the 2d-reference potential for protonated diglyme was calculated for the collinear proton transfer only because a fully relaxed 3-dimensional PES for protonated diglyme would be computationally very demanding.

B. Molecular Dynamics Simulations and Analysis. All molecular dynamics simulations were carried out with CHARMM[34] and the CHARMM22 force field.[47] The time step used was 0.25 fs, sufficiently small to follow the rapid hydrogen motions and to ensure energy conservation. The systems ($H_5O_2^+$ and protonated diglyme) were heated and equilibrated at the target temperatures (5, 10, 25, 50, and 100 K) for 5 ps. All production MD simulations were 125 ps in length and all atoms were free to move.

MD simulations were started from the optimized ab initio structures. The atom types and force constants are taken from the CHARMM22 force field and are summarized in Table 2 together with the force field parameters in Table 3. The parametrization of water corresponds to the TIP3P force field with a modified OH force constant ($k_{OH} = 550$ (kcal/mol)/Å^2) to reproduce the frequency of the symmetric O−H stretching vibration.

Shared Protons in Different Chemical Environments

J. Phys. Chem. A, Vol. 111, No. 9, 2007 **1641**

TABLE 3: Force Field Parameters for Bonded and Nonbonded Interactions for $H_5O_2^+$ and Protonated Diglyme from the CHARMM22 Force Field[47]

	bond			angle			dihedral				nonbonded		
atoms	k	r_e/Å	atoms	k	θ_e/deg	atoms	k	n	ϕ_e/deg	atoms	ϵ (kcal/mol)	σ/Å
						$H_5O_2^+$							
O H	550.0	0.9572	H O H	55.0	104.52					H	−0.046	0.2245
										O	−0.1521	1.7682
						Protonated Diglyme							
O C	450.0	1.45	H OH C	50.0	120.0	OH C C H	0.25	2	180.0	H	−0.046	0.2245
OH C	450.0	1.45	C O C	50.0	130.0	O C C H	0.25	2	180.0	O	−0.12	1.7
OH H	450.0	1.00	C OH C	50.0	120.0	H C C H	0.25	2	180.0	OH	−0.12	1.7
C C	450.0	1.45	C C O	50.0	140.0	C O C H	0.25	2	180.0	C	−0.11	2.0
C H	320.0	1.10	C C H	35.0	110.0	C OH C C	0.25	2	180.0			
			O C H	35.0	110.0	C O C C	0.25	2	180.0			
			C C OH	50.0	140.0	OH C C O	0.25	2	180.0			
			C O H	60.0	115.0	H OH C C	0.25	2	180.0			
			H C H	35.0	109.0	C OH C H	0.25	3	180.0			
			OH C H	50.0	109.0	H C OH H	0.25	3	180.0			

MD simulations provide coordinates and the total dipole moment of the system as a function of time t. Infrared spectra are calculated from the Fourier transform of the dipole−dipole autocorrelation function. To this end, the total dipole moment $M(t)$ recorded along the trajectory, was correlated over 2^{15} time origins to give $C(t)$. Using a Blackman filter[48] to suppress noise and a fast Fourier transform, the spectral signal $C(\omega)$ is obtained. To arrive at the infrared spectrum $A(\omega)$, the function $C(\omega)$ is weighted with the correct Boltzmann weight[49,50]

$$A(\omega) = \omega\{1 - \exp[-\omega/(kT)]\}C(\omega) \qquad (8)$$

where ω is the frequency, k is the Boltzmann constant, and T is the temperature in Kelvin. The resolution of the spectra is 2 cm^{-1}.

In a conventional force field calculation the total dipole moment $M(t)$ is calculated from the atom-centered partial charges of the atoms. For the present simulations two possibilities were explored. In the first one, partial charges from a natural bond order (NBO) analysis[51] were calculated on the energy minimized structure for $H_5O_2^+$ and protonated diglyme, respectively, using the electronic structure methods mentioned above. Second, for protonated water dimer the fully (15-)dimensional dipole moment surface of Huang et al.[52] was used to calculate $M(t)$ from the coordinates along the trajectory.

For the MD simulations of protonated water dimer no partial charges were assigned to the atoms to avoid double counting of electrostatic interactions. This is not appropriate for protonated diglyme. Here we used scaled NBO partial charges in the MD simulations. The scaling was determined such as to reproduce the B3LYP/6-311++G(d,p) energies together with the morphing as closely as possible. A factor of 1/10 was found to be appropriate (see Figure 2C).

III. Results

For both systems five independent MD simulations, 125 ps in length, were run at each temperature and averaged subsequently. The dynamics of the systems is analyzed using the atomic trajectories, the dipole−dipole time correlation functions and the corresponding infrared spectra. Power spectra for all internal motions of interest are calculated from the associated time series. These motions include the O−O stretch, the O−H* stretch, and the O−H*−O bending vibrations. The power spectra can be used to reveal couplings between the different degrees of freedom.

A. Energetics, Power, and Infrared Spectra from MMPT/ MD Simulations. *Protonated Water Dimer.* The minimum

energy structure of $H_5O_2^+$ from MP2/6-311++G(d,p) calculations is shown in Figure 1a. The O−O equilibrium distance is $R_{eq} = 2.38$ Å with $\rho_{eq} = 0.5$ and a slightly nonlinear structure $\theta_{O-H^*-O} = 177°$. This is in agreement with other, higher-level ab initio calculations.[52−54] The calculated MP2/6-311++G(d,p) ab initio energies (Figure 2A1) and the fitted PES (Figure 2A2) for $\theta = 0$ are shown together in Figure 2D. The fit of the functional form to the ab initio points is satisfactory.

The infrared spectrum of $H_5O_2^+$ and DH$_4O_2^+$ at $T = 5$ K (see Figure 3) was evaluated from the coordinates along the trajectories with the 15-dimensional dipole moment surface of Huang et al.[52] Spectral lines were assigned to particular motions using normal mode calculations and comparison between the H*- and D*-containing species (black and red curves, respectively). The OHO water bend is barely shifted (1772 cm^{-1} for $H_5O_2^+$ and 1767 cm^{-1} for DH$_4O_2^+$), because the transferring H*/D* atom is essentially not involved in this mode. At lower frequency, small, broad features appear at 1332 and 1260 cm^{-1} (center frequencies) for $H_5O_2^+$, which shift to 1126 and 1060 cm^{-1} upon deuteration. This corresponds to deuteration shifts of 1.19. Using normal-mode analysis and the power spectra (Figure 4) of intermolecular coordinates, these bands are assigned to (O−H*−O)$_{x,y}$ bending vibrations. However, the power spectra (Figure 4) suggest that the two modes are coupled to other modes. The peaks at 890 and 856 cm^{-1} are essentially unshifted between the two isotopically substituted molecules and correspond to H_2O torsion coupled to the O−O stretch. At 724 cm^{-1} the asymmetric OH*O stretch appears, which is shifted down to 521 cm^{-1} upon deuteration. This is a deuteration shift of 1.39. At even lower wavenumbers (438 and 389 cm^{-1}, respectively), collective bending vibrations involving the bridging H*/D* atom appear.

Compared to the harmonic frequency from the MP2/6-311++G(d,p) calculations (899 cm^{-1}), the asymmetric OH*O stretch frequency is shifted considerably to the red (724 cm^{-1}), which amounts to a relative shift of 24%. There are a number of factors that potentially contribute to this observation. First, the asymmetric OH*O coordinate has a substantial anharmonicity that will lower the frequency. As a comparison, in the ionic complex He−HCO$^+$ the intermolecular stretching frequency (He stretch) calculated from the second derivative of the potential at the minimum is found at 140 cm^{-1} (MP2/aug-cc-pVTZ) whereas the anharmonic value is at 87 cm^{-1}.[55] For a much more strongly bound system such as Ar−HCO$^+$ the harmonic[56] and anharmonic[57] frequencies along the intermolecular stretching coordinate are 149.4 and 132.8 cm^{-1}, respectively. Thus, in these cases anharmonicity leads to a reduction
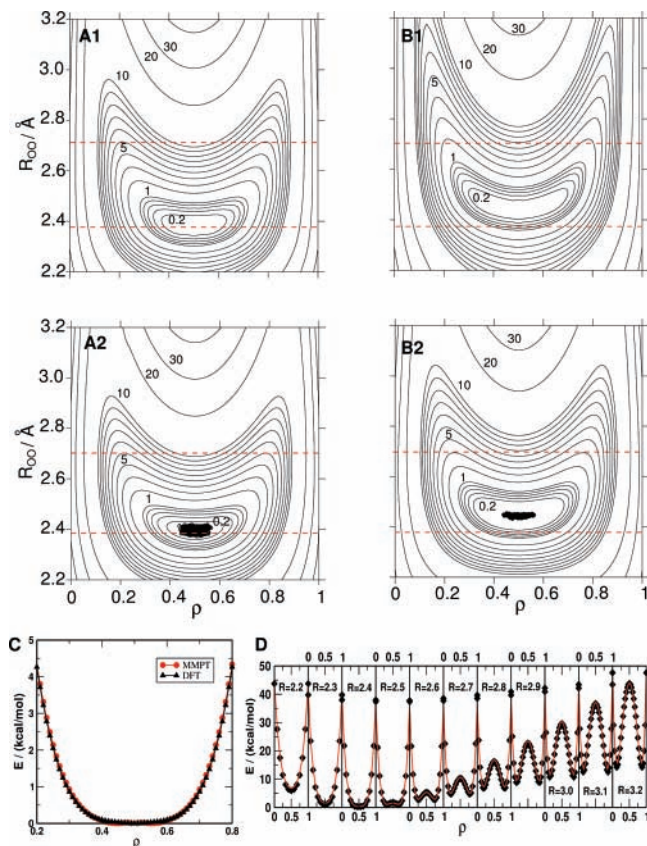
Figure 2. (A1) Relaxed PES scan from MP2/6-311++G(d,p) calculations for the hydrogen bridge for oxygen–oxygen distances R_{OO} from 2.2 to 3.2 Å and ρ ranging from 0 to 1 and $\theta = 0°$ for $H_5O_2^+$. The minimum energy is found at $R = 2.38$ Å and $r = 1.19$ Å (i.e., $\rho = 0.5$). (A2) Fitted PES from the analytical energy function using the fitted parameters (eqs 2–7 and Table 1). (B1) PES along the PT coordinates (R,ρ) for protonated diglyme from B3LYP/6-311++G(d,p) calculations. (B2) MMPT (morphed potential of (A2)) with $\lambda_1 = 1.025$ (shift of equilibrium geometry) and $\lambda_2 = 0.95$ (flattening of the PES). Contours are drawn every 0.2 kcal/mol up to 1 kcal/mol, then every 1 kcal/mol up to 10 kcal/mol, and at 20 kcal/mol and 30 kcal/mol. The dashed red lines guide the eye to compare the two sets of surfaces. They cross through the minimum of the $H_5O_2^+$ potential and through the line at 5 kcal/mol at long range. Computationally, (A1) and (B1) correspond to the "expensive" PESs and (A2) and (B2) are rapid to evaluate. (A2) and (B2) also show the phase space sampled by a typical trajectory at 50 K. (C) Comparison of the B3LYP/6-311++G(d,p) potential and the MMPT potential for $R_{OO} = $ constant through the minimum of the respective PES. (D) Calculated MP2/6-311++G(d,p) energies (diamonds) for $H_5O_2^+$ and fitted (solid line) analytical form for the PES as a function of ρ for 11 cuts $R = $ constant and for $\theta = 0$. Energies are in kcal/mol.

of the harmonic value of 60% and 13% for the He and Ar-containing complex, respectively, which brackets the value for the asymmetric OH*O stretch in $H_5O_2^+$. A second reason for the difference between the harmonic and anharmonic values is related to the accuracy of fitting the ab initio energies. Although the fit is satisfactory, small inaccuracies will affect the vibrational frequencies and lead to differences between ab initio calculations and the surfaces derived from them. Finally, the coupling between the various degrees of freedom in the quantum chemical calculations is likely to differ from the ones in the MMPT potential.

For comparison with experimental data, simulations at higher temperatures are more relevant. Thus, the infrared spectra of $H_5O_2^+$ (black) and $DH_4O_2^+$ (blue) were also calculated at 50 K. They are shown together with power spectra for selected
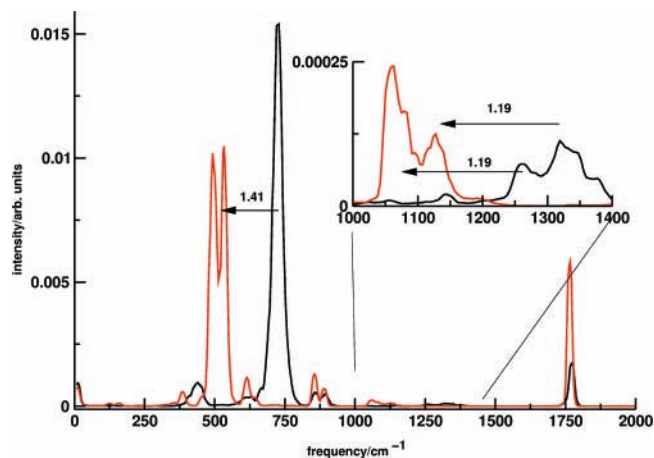
Figure 3. Averaged infrared spectra for $H_5O_2^+$ (black trace) and $DH_4O_2^+$ (red trace) from MMPT/MD simulations at 5 K. The spectra are calculated from the 15-dimensional dipole moment surface by Huang et al. (see text)[52] and averaged over 5 runs. Isotope shifts are given as horizontal arrows. The inset shows a magnification of signal in the bending region (see Table 4) with corresponding isotope shifts. The HOH bending mode is essentially unshifted. All spectra are normalized to unity.
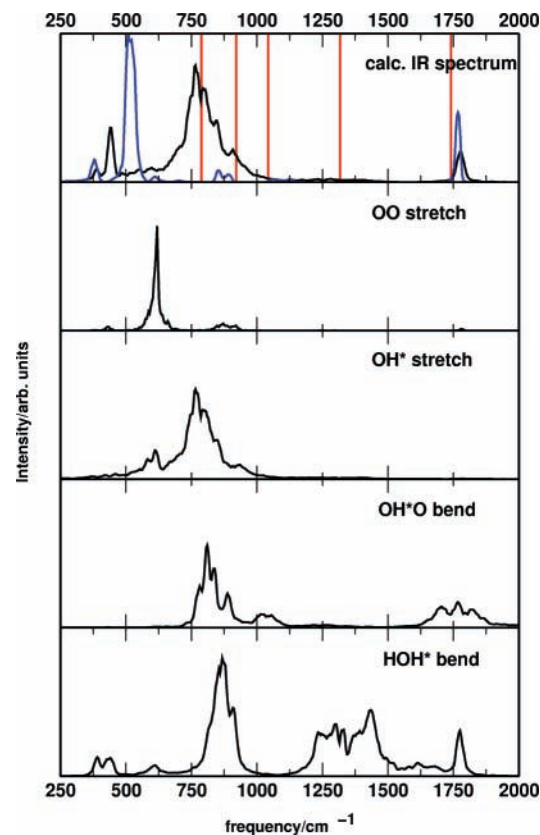
Figure 4. Averaged infrared spectra for $H_5O_2^+$ (black) and $DH_4O_2^+$ (blue) at 50 K (top panel) together with the experimental line positions (red bars for wavenumbers). The four lower panels show the averaged power spectra of the O–O and OH* stretching vibrations and the OH*O and HOH* bending vibrations, respectively.

coordinates of $H_5O_2^+$ in Figure 4. Most experimental line positions (red bars), at 750, 900, 1330, and 1770 cm^{-1}, correspond to features in the calculated infrared spectra. The power spectra for the different coordinates are useful to detect couplings between different modes. Figure 4 shows that motion along the O–H* coordinate (involved in the O–H*–O asymmetric stretch) is coupled to the O–O stretching and the OH*O

Shared Protons in Different Chemical Environments

J. Phys. Chem. A, Vol. 111, No. 9, 2007 **1643**

TABLE 4: Comparison of Harmonic (Upper Half) and Anharmonic Frequencies (Lower Half) for Stretching and Bending Modes Involving the Transferring H* and the Symmetric O−O Stretching Vibration in $H_5O_2^{+a}$

	Harmonic Vibrational Frequencies			
mode	ref 54 BCCD(T)/TZ2P	refs 53, 52 OSS3(p)	ref 52 CCSD(T)/a-VTZ	this work MP2/6-311++G(d,p)
O−O stretch	650	688	630	633
OH*O_{as} stretch	794	857	861	899
OH*O_x bend	1505	1486	1494	1516
OH*O_y bend	1596	1505	1574	1564
	Anharmonic Vibrational Frequencies			
mode	OSS3(p) VCI (15d)[21]	OSS3(p) CFQMC[29]	CCSD(T)/a-VTZ MD 100 K[23]	MMPT MD 100 K
O−O stretch	569	516 ± 4	630[b]	617
OH*O_{as} stretch	902	737 ± 3	861[b]	830
		870 ± 6		
OH*O_x bend	1354	n.a.	n.a.	1266
OH*O_y bend	1388	n.a.	n.a.	1321

[a] Data from the literature and the present calculations are compared. The two states for the asymmetric O−H*−O stretch from the CFQMC calculations contain a significant amplitude along this mode.[29] For the anharmonic frequencies, the first header refers to the interaction potential and the second line to the method to calculate the vibrational frequencies. n.a. labels states for which no assignment has been made in the respective works. Frequencies are given in cm^{-1}. [b] The MD simulations in ref 23 do not give the anharmonic frequencies themselves but the overlap matrix between the driven frequencies with the normal modes. For example, driving at 860 cm^{-1} leads to considerable overlap with the normal mode at 861 cm^{-1} and some overlap with the mode at 630 cm^{-1}.

and HOH* bending coordinate. Together with the infrared spectrum, the power spectra are used to approximately assign the vibrational band. In addition to the assignments made in the previous paragraph, the O−O mode is found at 617 cm^{-1}, which agrees quite favorably with 630 cm^{-1} from MD simulations on the CCSD(T)/aug-cc-pVTZ surface.[23] It is also observed that the infrared spectrum does not show a band around 600 cm^{-1}. This is expected because the symmetric O−O stretch is infrared inactive.

Table 4 presents harmonic and anharmonic frequencies for the O−O symmetric and the O−H*−O asymmetric stretch and the two O−H*−O bending vibrations. Data are shown from BCCD(T)/TZ2P calculations[54] and calculations on the OSS3-(p) PES,[52,53] the most recent CCSD(T)/aug-cc-pVTZ PES,[52] and MP2/6-311++G(d,p), the method used for the MMPT potential. All harmonic frequencies agree fairly well. However, their value in understanding the experimental spectra is very limited because of the anharmonicities and the flat PES along different coordinates. The lower part of Table 4 compares anharmonic frequencies calculated on the OSS3(p) PES using 15-dimensional vibrational configuration interaction (VCI)[21] or quantum Monte Carlo (CFQMC) calculations[29] along with MD simulations on the CCSD(T)/aug-cc-pVTZ[23] and the MMPT (this work) potential energy surfaces at 100 K. The O−O stretching vibration on the OSS3(p) is lower by about 50−100 cm^{-1} compared to the other two PESs whereas the two MD simulations give quite similar results. For the O−H*−O asymmetric stretch QMC calculations on the OSS3(p) PES yield two modes with considerable O−H*−O amplitude (737 and 870 cm^{-1}) whereas the VCI calculations find one mode at 902 cm^{-1}. Although Cho and Singer[29] and Dai et al.[21] use the same PES it is not clear which of the two asymmetric O−H*−O stretch bands from the CFQMC calculations correspond to the one found in the VCI calculations. Finally, O−H*−O bending vibrations from VCI and MD simulations are in the 1300 cm^{-1} region. It was previously found[30] that, depending on the method and the PES, the splitting between the (O−H*−O)$_x$ and (O−H*−O)$_y$ bend ranges from 11 to 58 cm^{-1}, which agrees with 55 cm^{-1} from the actual simulations. The almost quantitative agreement with MD simulations on the 15-dimensional CCSD-(T) surface and the fair agreement with different calculations

on the OSS3(p) potential suggest that the MMPT surface is of sufficiently high quality to serve as a zeroth-order approximation for morphing and for use in a related system such as protonated diglyme.

Protonated Diglyme. The fully relaxed B3LYP/ 6-311++G(d,p) PES along R and ρ is shown in Figure 2B1. It exhibits a faint double-minimum structure with a barrier for PT below 0.2 kcal/mol. Constraining the molecule at its MP2/6-311++G(d,p) optimized geometry, this barrier is 1.2 kcal/mol, which is an upper limit at this level of theory and is considerably lower than the previously reported value of 4.6 kcal/mol.[8] Comparison of the PES for protonated diglyme and for $H_5O_2^+$ shows that at large R the PES is flatter for the former. Because the topologies of the two PESs shown in Figure 2A1,-B1 are similar, a 3-dimensional PES for describing PT in protonated diglyme can be derived from the PES for proton transfer in $H_5O_2^+$ in the following way. In the spirit of the original morphing[33] and previous PES-scaling approaches,[58] the surface for proton transfer in $H_5O_2^+$ is used as a zeroth-order approximation and related to PT in protonated diglyme via the transformation $\tilde{V}_{diglyme}(R,\rho,\theta) = \lambda_1 V(\lambda_2 R,\rho,\theta)$. To determine approximate morphing parameters, the fully relaxed B3LYP/6-311++G(d,p) PES along $V(R,\rho,\theta{=}0)$ serves as the reference.

The most obvious difference between the B3LYP/6-311++G(d,p) PES for protonated diglyme and the MP2/6-311++G(d,p) PES for protonated water (compare Figure 2B1 and Figure 2A1) is the location of the O−O minimum (2.38 Å in $H_5O_2^+$ compared to 2.43 Å in protonated diglyme) and the curvature around the minimum: for protonated diglyme the interaction potential is flatter than that for $H_5O_2^+$ at large R. By applying $\tilde{R} = \lambda_1 R$ and $\tilde{E} = \lambda_2 E$ with $\lambda_1 = 1.025$ and $\lambda_2 = 0.95$ to the protonated water dimer PES, we can transform it into a PES suitable for describing PT in protonated diglyme. This is the MMPT PES for protonated diglyme. Parts B1 and B2 of Figure 2 compare the B3LYP/6-311++G(d,p) PES and $\tilde{V}_{diglyme}(R,\rho,\theta)$. Around the minimum, the region probed by the MD simulations, the two PESs are very similar (see Figure 2C, which compares the two PESs for R_{OO}^{min}, i.e., the cut for $R_{OO} =$ constant through the minimum of the respective PES) but for larger R the curvature of the morphed PES differs from
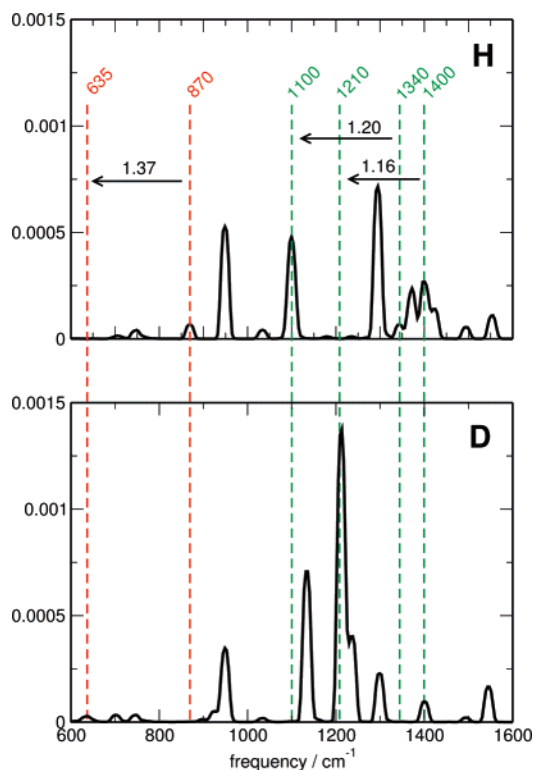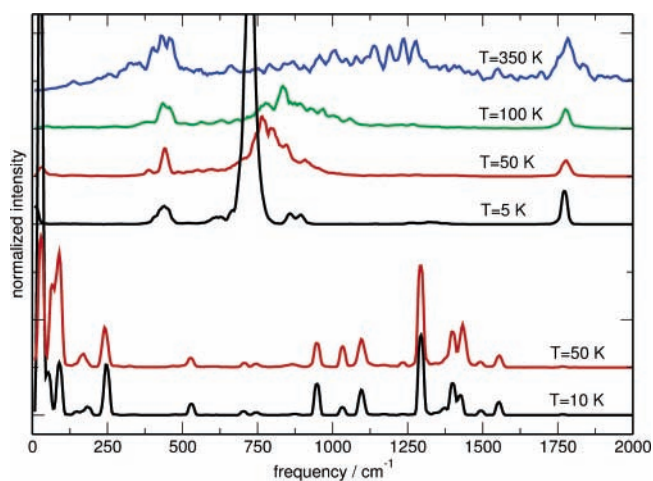
Figure 5. Averaged infrared spectra for protonated diglyme from MMPT/MD simulations at 1 K. Spectra for different masses of the transferring particle (m_{H*} = 1.008 amu, m_{D*} = 2.016 amu) and lines connecting corresponding peaks are shown. Energies are in cm^{-1}, and intensities in arbitrary units. The red dashed lines are for spectral features corresponding to the OH*O asymmetric stretch, and the green dashed lines are for the bending modes that are present in the [diglyme-H]$^+$ and in [diglyme-D]$^+$, respectively. Deuteration shifts are indicated by horizontal arrows.

the B3LYP/6-311++G(d,p) PES. Once sufficient reference data are available, a more detailed morphing can be envisaged. However, the dynamics on PES (B2) shows that motion along R is restricted to the phase space enclosed by the 0.2 kcal/mol contour, i.e., $R \leq 2.5$ Å, which is the region where (B1) and (B2) are very similar.

Molecular dynamics simulations for protonated diglyme ([diglyme-H]$^+$ and [diglyme-D]$^+$) were run using the morphed $\tilde{V}_{diglyme}(R,\rho,\theta)$ for the transferring proton/deuteron. From the total dipole moment $M(t)$ is the infrared spectrum and power spectra along coordinates relevant for proton transfer were calculated. The power spectra reveal considerable coupling between the different modes. For better assignments, in particular of the modes involving the bridging proton H*, spectra were calculated at low temperature (1 K, see Figure 5). To assist the assignments of the lines, MD simulations were carried out by varying the mass of the transferring particle between 1 and 2 amu in steps of 0.2 amu. The averaged spectra display a number of lines that exclusively appear in the hydrogenated and deuterated species, respectively. First the asymmetric OH*O stretching vibration is assigned. With increasing mass of the transferring particle the band at 870 cm^{-1} shifts progressively down to 635 cm^{-1}. Furthermore, comparison of the power spectra (as was done for H$_5$O$_2^+$, see Figure 4) of the OH* and OD* stretching coordinates establishes this assignment. The deuteration shift for the asymmetric OH*O stretch is 1.37, somewhat lower than for the protonated water dimer (1.39).

Additional sets of lines (1340 and 1400 cm^{-1}) and (1100 and 1210 cm^{-1}) have deuteration shifts of 1.20 and 1.16, compared

Figure 6. Infrared spectra for H$_5$O$_2^+$ (upper four traces) and protonated diglyme (lower two traces) from MMPT/MD simulations. Temperature effects are found to be small for protonated diglyme, but they are more pronounced for H$_5$O$_2^+$. Energies are in cm^{-1}, and intensities in arbitrary units. The quality of the dipole moment surface for H$_5$O$_2^+$ and [diglyme-H]$^+$ is not comparable (see text).

to shifts of 1.19 for OH*O bending modes in H$_5$O$_2^+$. Their assignment to OH*O bending motions is not as firm as for the asymmetric OH*O stretch. Starting from the blue end of the spectrum, the two lines above 1450 cm^{-1} are not influenced by isotopic substitution and thus are not involved in either H* stretching or bending motion. Conversely, the congested spectral pattern around 1400 cm^{-1} in [diglyme-H]$^+$ has only one line in the deuterated species. Thus, the pattern around 1400 cm^{-1} must be related to H* motion. Deuteration shifts of H-bending vibrations are expected between 1.1 and 1.2. A comparison of the two spectra in Figure 5 shows that the lines at 1210 and 1100 cm^{-1} in [diglyme-D]$^+$ have no companion in the [diglyme-H]$^+$ spectrum. This suggests the correspondence as indicated in Figure 5. Normal-mode analysis based on both the MMPT surface and the optimized B3LYP/6-311++G(d,p) level confirm that these lines involve the OH*O in-plane bending vibration which is, however, strongly mixed with other degrees of freedom. The relative intensities of the lines differ partly due to the simplified model used for the dipole moment (see, e.g., the lines at 1500 and 1550 cm^{-1}). Further experiments on the deuterated species will help in the assignment of the lines.

B. Comparison of the MMPT/MD Simulations for H$_5$O$_2^+$ and Protonated Diglyme. Figure 6 shows IR spectra for H$_5$O$_2^+$ at 5, 50, 100, and 350 K (calculated from 5 trajectories) and for protonated diglyme at 10 and 50 K. It is apparent that the spectra of H$_5$O$_2^+$ are considerably more affected by temperature than the ones for protonated diglyme. The temperature dependence of the H$_5$O$_2^+$ spectra has already been found previously.[23,31]

The dominant asymmetric stretching vibrations are at different frequencies in H$_5$O$_2^+$ and in [diglyme-H]$^+$. In H$_5$O$_2^+$ the O−H*−O asymmetric stretching vibration shifts from 724 cm^{-1} (at 5 K) to 830 cm^{-1} (at 100 K) whereas it is at 870 cm^{-1} in protonated diglyme at all temperatures investigated. One possible explanation for this observation is that the molecular scaffold couples differently to the PT motif in protonated diglyme compared to that in H$_5$O$_2^+$, i.e., that the relatively free motion of the water molecules along the OH*O motif in H$_5$O$_2^+$ has a different influence on the spectroscopy than the more con-strained motion of H* in the H$_3$C−CH$_2$O−H*−OCH$_2$−CH$_3$ motif in [diglyme-H]$^+$ (see Figure 1). The coupling between stretch and bending vibrations to the OH*O asymmetric stretch

Shared Protons in Different Chemical Environments

J. Phys. Chem. A, Vol. 111, No. 9, 2007 **1645**
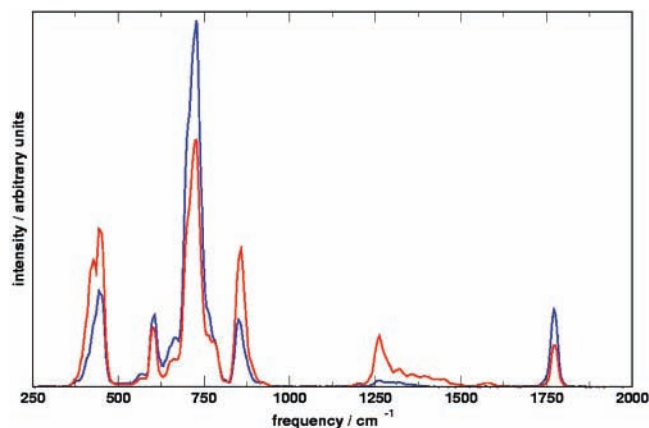
Figure 7. Averaged infrared spectra for $H_5O_2^+$ at 10 K calculated from atom-centered, partial NBO charges (red curve) and from the 15-dimensional dipole moment surface (blue curve). The positions of the lines are essentially identical whereas their intensities depend on the model from which $M(t)$ is calculated. This is particularly apparent for the region around 1300 cm^{-1}, which is related to the HOH* bending vibrations.

in [diglyme-H]$^+$ has been assessed through modifications of particular force field parameters. Possible candidates that can couple to the OH*O motion in [diglyme-H]$^+$ include the CO bond, and the COC and CCO valence angles (see Figure 1). The particular force constants (see Table 3) were varied by ± 10 % and the infrared spectrum was calculated as before. Compared to the center value ($k_{C-OH} = 450$ (kcal/mol)/Å^2), the band at 870 cm^{-1} shifts to 874 and 865 cm^{-1} for a stronger or weaker k_{C-OH}, respectively. Modifications of the angular force constants, which are typically weaker than the stretching force constants by a factor of 10, have smaller effects on the location of the OH*O asymmetric stretch. The same is observed for modifications of k_{COC}. In summary, the frequency of the asymmetric stretching motion in [diglyme-H]$^+$ is coupled to the environmental degrees of freedom but changes in the force constants by up to 10% shift the frequency by no more than 10 cm^{-1}.

IV. Discussion and Conclusion

In this work, the MMPT potential has been used to investigate proton transfer dynamics and to characterize the infrared spectra of $H_5O_2^+$ and protonated diglyme. The MMPT potential allows to investigate the long-time (several 100 ps) bond-breaking and bond-forming (i.e., reactive) dynamics that are similar to those of mixed QM/MM MD simulations. The vibrational spectra were calculated from the dipole–dipole autocorrelation function, and assignments were made using simulations with deuterated species and power spectra calculated along the most relevant coordinates. For protonated water dimer a state-of-the art 15-dimensional dipole moment surface[52] was used to calculate the infrared spectrum, but for [diglyme-H]$^+$ only a point charge model is available. The quality of the MMPT PES for $H_5O_2^+$ was validated by comparing vibrational excitations with previous MD, DMC, and VCI calculations on high-quality PESs. The results suggest that the MMPT PES is suitable as a zeroth-order approximation for other proton transfer motifs of the form XO···H$^+$···OX, such as in protonated diglyme. The recent MD simulations by Bowman and co-workers on a high-quality, 15-dimensional PES bear most similarities with the present investigation.[52] For 100 K they find the asymmetric O–H*–O stretching vibration (possibly coupled with a torsional mode) at 860 cm^{-1}, which agrees favorably with the 830 cm^{-1} at the same temperature calculated with the MMPT potential. Fur-

thermore, the infrared inactive symmetric OH*O stretching vibration is found at 620 cm^{-1} (see Figure 4) whereas Bowman et al. find it at 630 cm^{-1}.[23] Deuteration shifts for the vibrations involving the transferring H* are 1.39 and 1.19 for the asymmetric O–H*–O stretching and bending modes from MMPT/MD simulations, which compares with 1.33 and 1.25 from VCI calculations on the OSS3(p) PES.[21]

Meaningful ab initio MD simulations for protonated diglyme at the correlated level (e.g., MP2) are beyond current computing power, and probably remain so for the foreseeable future. Even calculating and fitting a relaxed 3d PES for protonated diglyme at the B3LYP/6-311++G(d,p) level would be extremely laborious. Thus, alternative computational methodologies beyond the harmonic approximation are required to follow the proton motion and to understand the associated spectroscopy in a system such as [diglyme-H]$^+$. Here, the intermolecular potential was formulated in a manner inspired by mixed QM/MM methods and an approximate energy- and coordinate-scaling was applied to the 3d PES for $H_5O_2^+$ to reproduce the shape and major features of the 2d relaxed PES for protonated diglyme. This morphed PES was subsequently used in long MD simulations. For [diglyme-H]$^+$ a one-to-one comparison of the vibrations with assignments from experiment is difficult. This is mainly because coupling between modes leads to mixing between "pure'' O···H$^+$···O asymmetric stretch and in- or out-of-plane bend modes decoupled from other framework vibrations. From careful analysis and comparison with simulations of the deuterated species, the bands at 870, 1340, and 1400 cm^{-1} are assigned to the O···H$^+$···O asymmetric stretch and in-plane bending modes, respectively. For the O···H$^+$···O asymmetric stretch this compares with frequencies between 724 and 830 cm^{-1} in $H_5O_2^+$, depending on the temperature. Thus, it is possible that the experimentally observed spectral features for protonated diglyme below 800 cm^{-1} indeed belong to the O···H$^+$···O asymmetric stretch.[8]

It is possible that quantum effects, in particular proton tunneling and zero-point effects, modify the spectra. On the other hand, it has previously been shown that although classical MD simulations neglect quantum effects, they are useful for interpreting vibrational spectra of molecular species.[23] Quantum effects are expected to play an important role at low temperature. However, most of the vibrationally resolved spectra that probe the H$^+$ transfer region are from studies with high laser power.[6–8] As such, the measured spectra likely involve fairly hot species with considerable amounts of internal energy where quantum effects are usually found to be of minor importance. Even studies under relatively mild experimental conditions found internal temperatures between 130 and 170 K in NH$_4^+$(H$_2$O)$_n$ clusters for ($n \leq 6$).[59]

The advantage of the present simulations is that they take the full dimensionality of the phase space into account. For strongly bound clusters and molecules temperatures can be derived from the widths of rotational line profiles and the assignment of hot bands. However, for a floppy system such as $H_5O_2^+$ with a strongly anharmonic potential the available phase space and the effective potential on which the dynamics takes place can change as a function of temperature. The shifting and broadening of vibrational bands associated with H$^+$ displacement has been previously found in classical MD spectra of $H_5O_2^+$ [23,31] and is confirmed by the present simulations. This is in contrast to protonated diglyme where, as expected, no temperature dependence of the vibrational bands is found. Linear extrapolation of the band maximum of the asymmetric O–H*–O stretch in $H_5O_2^+$ from Figure 6 to 921 cm^{-1} yields $T \approx 200$ K,

which is somewhat higher than previously estimated temperatures in supersonic jets.[59] A more recent study of the infrared spectroscopy of larger protonated water clusters has estimated the excess internal energy in the $H^+[H_2O]_{21}$ cluster to be around 1.5 eV, which amounts to 270 K per soft degree of freedom.[60]

It is of interest to compare the IR spectra calculated from the fully dimensional dipole moment surface[52] and from a simpler point-charge description. To this end, five additional MD simulations at 10 K were carried out for $H_5O_2^+$ and $M(t)$ was calculated from these trajectories using the two different models. The averaged spectra are shown in Figure 7. It is found that the positions of the lines are essentially identical whereas the relative intensities can differ considerably. In particular, the region around 1300 cm^{-1} appears far more intense using the NBO charges. This suggests that the potential energy surface largely determines the location of the spectral lines whereas accurate knowledge of the dipole moment surface provides realistic relative intensities.

Previously, the "morphing potential" approach has been successfully used for complexes such as Ne−HF, Ar−HBr, or He−OCS.[33,42,61] It is important to stress that the final potential is an *effective* potential which means for the above systems that it is only valid for the frozen monomer configuration (e.g., HF bond length in Ne−HF) chosen. This is also true for the present work. Once firm assignments are available, the MMPT potential for $H_5O_2^+$ itself can be systematically improved to optimally reproduce the experimental observables and will yield an effective MMPT surface that is valid for the force field parameters chosen. In the present work we applied the morphing procedure in a slightly different manner, namely to approximately morph an initial PES to reproduce the ab initio surface for proton transfer in protonated diglyme. The morphed surface was then used to explore the vibrational states of the molecule. It is of interest to mention that the present approach should also be suitable to investigate systems in the condensed phase. For example, it is possible to solvate the system in question (e.g., protonated water dimer) and to calculate its spectroscopic properties from an MD simulation. Comparison with experimental data will provide the necessary data to apply the morphing procedure. This will involve iterative, nonlinear least-squares fitting of the calculated values to the experimental data.

In summary, the present work reports computational studies of the relationship between the infrared spectra for $H_5O_2^+$ and [diglyme-H]$^+$ in view of their common proton transfer motif. The underlying PES is suitable to describe proton transfer and is based on a morphed, 3-dimensional PES that explores the similarity between $H_5O_2^+$ and protonated diglyme. The MMPT surface for $H_5O_2^+$ was validated against recent MD simulations. Comparison of the infrared spectra of [diglyme-H]$^+$ and $H_5O_2^+$ shows that there is not necessarily a straightforward relationship between these spectra that would allow for an assignment of the bands. Based on the present investigations, it is, however, possible that the experimentally observed feature below 800 cm^{-1} corresponds to the asymmetric O−H*−O stretch. It is also found that, as expected, the infrared spectrum of [diglyme-H]$^+$ is largely unaffected by temperature whereas the bands in $H_5O_2^+$ considerably shift and broaden. For the as yet unobserved infrared spectrum of [diglyme-D]$^+$ a deuteration shift of 1.37 for the asymmetric OH*O stretch is predicted. Experimental studies of [diglyme-D]$^+$ would be useful to test this proposition.

References and Notes

(1) von Grotthus, C. *Ann. Chim.* **1806**, *LVIII*, 54.
(2) Eigen, M. *Ang. Chem. Intern.* **1964**, *3*, 1−19.
(3) Pratt, D. W. *Annu. Rev. Phys. Chem.* **1998**, *49*, 481−530.
(4) Folmer, D. E.; Wisniewski, E. S.; Hurley, S. M.; Castleman, A. W. *Proc. Natl. Acad. Sci. U.S.A.* **1999**, *96*, 12980.
(5) Bach, A.; Leutwyler, S. *J. Chem. Phys.* **2000**, *112*, 560.
(6) Asmis, K. R.; Pivonka, N. L.; Santambrogio, G.; Brümmer, M.; Kaposta, C.; Neumark, D. M.; Wöste, L. *Science* **2003**, *299*, 1375.
(7) Fridgen, T. D.; McMahon, G. B.; MacAleese, L.; Lemaire, J.; Maitre, P. *J. Phys. Chem. A* **2004**, *108*, 9008.
(8) Moore, D. R.; Oomens, J.; van der Meer, L.; von Helden, G.; Meijer, G.; Valle, J.; Marshall, A. G.; Eyler, J. R. *Chem. Phys. Chem.* **2004**, *5*, 740.
(9) Hammer, N. I.; Diken, E. G.; Roscioli, J. R.; Johnson, M. A.; Myshakin, E. M.; Jordan, K. D.; McCoy, A. B.; Huang, X.; Bowman, J. M.; Carter, S. *J. Chem. Phys.* **2005**, *122*, 244301.
(10) Bueker, H.-H.; Helgaker, T.; Ruud, K.; Uggerud, E. *J. Phys. Chem.* **1996**, *100*, 15388.
(11) Wei, D.; Salahub, D. R. *J. Chem. Phys.* **1997**, *106*, 6086.
(12) Sagnella, D. E.; Tuckerman, M. E. *J. Chem. Phys.* **1998**, *108*, 2073.
(13) Vuilleumier, R.; Borgis, D. *J. Chem. Phys.* **1999**, *111*, 4251.
(14) Vener, M. V.; Kühn, O.; Sauer, J. *J. Chem. Phys.* **2001**, *114*, 240.
(15) Agmon, N. *Chem. Phys. Lett.* **1995**, *244*, 456.
(16) Pomes, R.; Roux, B. *J. Phys. Chem.* **1996**, *100*, 2519.
(17) Cheng, H.-P. *J. Chem. Phys.* **1996**, *105*, 6844.
(18) Day, T. J. F.; Schmitt, U. W.; Voth, G. A. *J. Am. Chem. Soc.* **2000**, *122*, 12027.
(19) Geissler, P. L.; Dellago, C.; Chandler, D.; Hutter, J.; Parrinello, M. *Chem. Phys. Lett.* **2000**, *321*, 225.
(20) Meuwly, M.; Karplus, M. *J. Chem. Phys.* **2002**, *116*, 2572.
(21) Dai, J.; Bacic, Z.; Huang, X.; Carter, S.; Bowman, J. M. *J. Chem. Phys.* **2003**, *119*, 6571.
(22) Fouqueau, A.; Meuwly, M. *J. Chem. Phys.* **2005**, *123*, 244308.
(23) Kaledin, M.; Kaledin, A. L.; Bowman, J. M. *J. Phys. Chem. A* **2006**, *110*, 2933.
(24) Mei, H. S.; Tuckerman, M. E.; Sagnella, D. E.; Klein, M. L. *J. Phys. Chem. B* **1998**, *102*, 10446.
(25) Liu, Y.; Tuckerman, M. E. *J. Phys. Chem. B* **2001**, *105*, 6598.
(26) Sadeghi, R. R.; Cheng, H.-P. *J. Chem. Phys.* **1999**, *111*, 2086.
(27) Lobaugh, J.; Voth, G. A. *J. Chem. Phys.* **1996**, *104*, 2056.
(28) See reference 14.
(29) Cho, H. M.; Singer, S. J. *J. Phys. Chem. A* **2004**, *108*, 8691.
(30) Sauer, J.; Döbler, J. *Chem. Phys. Chem.* **2005**, *6*, 1706.
(31) Cheng, H.-P.; Krause, J. L. *J. Chem. Phys.* **1997**, *107*, 8461.
(32) Hutson, J. M. *Annu. Rev. Phys. Chem.* **1990**, *41*, 123−154.
(33) Meuwly, M.; Hutson, J. M. *J. Chem. Phys.* **1999**, *110*, 8338.
(34) Brooks, B. R.; Bruccoleri, R. E.; Olafson, B. D.; States, D. J.; Swaminathan, S.; Karplus, M. *J. Comput. Chem.* **1983**, *4*, 187−217.
(35) Weiner, S. J.; Kollman, P. A.; Case, D. A.; Singh, U.; Ghio, C.; Alagona, G.; Profeta, Jr., S.; Weiner, P. *J. Am. Chem. Soc.* **1984**, *106*, 765.
(36) Warshel, A.; Levitt, M. *J. Mol. Biol.* **1976**, *103*, 227.
(37) Alagona, G.; Guio, C.; Kollman, P. A. *J. Mol. Biol.* **1986**, *191*, 23.
(38) Bash, P. A.; Field, M. J.; Karplus, M. *J. Am. Chem. Soc.* **1987**, *109*, 8092−8094.
(39) Field, M. J.; Bash, P. A.; Karplus, M. *J. Comput. Chem.* **1990**, *11*, 700.
(40) Warshel, A.; Weiss, R. M. *J. Am. Chem. Soc.* **1980**, *102*, 6218.
(41) Grochowski, P.; Lesyng, B.; Bala, P.; McCammon, J. A. *Int. J. Quant. Chem.* **1996**, *60*, 1143.
(42) Wang, Z.; McIntosh, A. L.; McElmurry, B. A.; Walton, J. R.; Lucchese, R. R.; Bevan, J. *J. Phys. Chem. A* **2005**, *109*, 8168−8179.
(43) Higgins, K. J.; Klemperer, W. *J. Chem. Phys.* **2005**, *122*, 244309.
(44) Frisch, M. J.; Trucks, G. W.; Schlegel, H. B.; Scuseria, G. E.; Robb, M. A.; Cheeseman, J. R.; Montgomery, J. A., Jr.; Vreven, T.; Kudin, K. N.; Burant, J. C.; Millam, J. M.; Iyengar, S. S.; Tomasi, J.; Barone, V.; Mennucci, B.; Cossi, M.; Scalmani, G.; Rega, N.; Petersson, G. A.; Nakatsuji, H.; Hada, M.; Ehara, M.; Toyota, K.; Fukuda, R.; Hasegawa, J.; Ishida, M.; Nakajima, T.; Honda, Y.; Kitao, O.; Nakai, H.; Klene, M.; Li, X.; Knox, J. E.; Hratchian, H. P.; Cross, J. B.; Bakken, V.; Adamo, C.; Jaramillo, J.; Gomperts, R.; Stratmann, R. E.; Yazyev, O.; Austin, A. J.; Cammi, R.; Pomelli, C.; Ochterski, J. W.; Ayala, P. Y.; Morokuma, K.; Voth, G. A.; Salvador, P.; Dannenberg, J. J.; Zakrzewski, V. G.; Dapprich, S.; Daniels, A. D.; Strain, M. C.; Farkas, O.; Malick, D. K.; Rabuck, A. D.; Raghavachari, K.; Foresman, J. B.; Ortiz, J. V.; Cui, Q.; Baboul, A. G.; Clifford, S.; Cioslowski, J.; Stefanov, B. B.; Liu, G.; Liashenko, A.; Piskorz, P.; Komaromi, I.; Martin, R. L.; Fox, D. J.; Keith, T.; Al-Laham,

Shared Protons in Different Chemical Environments

J. Phys. Chem. A, Vol. 111, No. 9, 2007 **1647**

M. A.; Peng, C. Y.; Nanayakkara, A.; Challacombe, M.; Gill, P. M. W.; Johnson, B.; Chen, W.; Wong, M. W.; Gonzalez, C.; Pople, J. A. *Gaussian 03*, revision C.01; Technical Report; Gaussian, Inc.: Wallingford, CT, 2004.

(45) Law, M. M.; Hutson, J. M. *Comput. Phys. Commun.* **1997**, *102*, 252.

(46) Lammers, S.; Meuwly, M. *Aust. J. Chem.* **2004**, *57*, 1223−1228.

(47) MacKerell, A. D., Jr.; et al. *J. Phys. Chem. B* **1998**, *102*, 3586.

(48) Harris, F. J. *Proc. IEEE* **1978**, *66*, 51.

(49) Schmitz, M.; Tavan, P. *J. Chem. Phys.* **2004**, *121*, 12233.

(50) Schmitz, M.; Tavan, P. *J. Chem. Phys.* **2004**, *121*, 12247.

(51) Reed, A. E.; Weinstock, R. B.; Weinhold, F. *J. Chem. Phys.* **1985**, *83*, 735.

(52) Huang, S.; Braams, B. J.; Bowman, J. M. *J. Chem. Phys.* **2005**, *122*, 044308.

(53) Ojamäe, L.; Shavitt, I.; Singer, S. J. *Int. J. Quant. Chem.* **1995**, *29*, 657.

(54) Valeev, E. F.; Schaefer, H. F., III. *J. Chem. Phys.* **1998**, *108*, 7197.

(55) Meuwly, M. *J. Chem. Phys.* **1999**, *110*, 4347.

(56) Dopfer, O.; Olkhov, R. V.; Maier, J. P. *J. Phys. Chem. A* **1999**, *103*, 2982.

(57) Buffa, G.; Dore, L.; Tinti, F.; Meuwly, M. *Chem. Phys. Chem.* **2006**, *7*, 1764.

(58) Gazdy, B.; Bowman, J. M. *J. Chem. Phys.* **1991**, *95*, 6309.

(59) Wang, Y. S.; Chang, H. C.; Jiang, J. C.; Lin, S. H.; Lee, Y. T.; Chang, H. C. *J. Am. Chem. Soc.* **1998**, *120*, 8777.

(60) Shin, J. W.; Hammer, N. I.; Diken, E. G.; Johnson, M. A.; Walters, R. S.; Jaeger, T. D.; Duncan, M. A.; Christie, R. A.; Jordan, K. D. *Science* **2004**, *304*, 1137.

(61) Howson, J. M. M.; Hutson, J. M. *J. Chem. Phys.* **2001**, *115*, 5059.